nature neuroscience

Synaptic inhibition of Purkinje cells mediates consolidation of vestibulo-cerebellar motor learning

Peer Wulff[1,7], Martijn Schonewille[2,7], Massimiliano Renzi[3], Laura Viltono[4], Marco Sassoè-Pognetto[4], Aleksandra Badura[2], Zhenyu Gao[2], Freek E Hoebeek[2], Stijn van Dorp[5], William Wisden[1,6], Mark Farrant[3] & Chris I De Zeeuw[2,5]

Although feedforward inhibition onto Purkinje cells was first documented 40 years ago, we understand little of how inhibitory interneurons contribute to cerebellar function in behaving animals. Using a mouse line (PC-Δγ2) in which GABA$_A$ receptor–mediated synaptic inhibition is selectively removed from Purkinje cells, we examined how feedforward inhibition from molecular layer interneurons regulates adaptation of the vestibulo-ocular reflex. Although impairment of baseline motor performance was relatively mild, the ability to adapt the phase of the vestibulo-ocular reflex and to consolidate gain adaptations was strongly compromised. Purkinje cells showed abnormal patterns of simple spikes, both during and in the absence of evoked compensatory eye movements. On the basis of modeling our experimental data, we propose that feedforward inhibition, by controlling the fine-scale patterns of Purkinje cell activity, enables the induction of plasticity in neurons of the cerebellar and vestibular nuclei.

Feedforward inhibitory microcircuits, in which interneurons and their target principal cells receive common excitatory input, enhance network performance in many brain regions[1,2]. In the hippocampus, feedforward inhibition, by reducing the time window of synaptic integration, increases the precision of spike timing in CA1 pyramidal neurons[3], and plasticity of feedforward inhibition is required to maintain the fidelity of information processing[4]. In the cerebellum, molecular layer interneurons (stellate and basket cells) control Purkinje cells by powerful feedforward inhibition[5–9] (**Supplementary Fig. 1**). In addition, subsets of Purkinje cells sparsely inhibit each other via axon collaterals[10]. Purkinje cells provide the only output of the cerebellar cortex and project to the cerebellar and vestibular nuclei. They fire complex spikes in response to climbing fiber activity[11] and simple spikes that reflect the integration of intrinsic pacemaker activity with excitatory and inhibitory synaptic inputs from parallel fibers and molecular layer interneurons[8,12–15].

Although feedforward inhibition onto Purkinje cells was documented more than four decades ago[5], we still know little about how it contributes to cerebellar function in behaving animals. Fast synaptic inhibition at molecular layer interneuron to Purkinje cell synapses is mediated by α1β2/3γ2-type GABA$_A$ receptors[16]. The γ2 subunit is required to target the receptors to the postsynaptic membrane[17]. To investigate the role of GABA$_A$ receptor–mediated feedforward inhibition, we selectively ablated the γ2 subunit, and thereby synaptic GABA$_A$ receptors, from Purkinje cells (PC-Δγ2 mice). The resulting changes that we observed in Purkinje cell simple-spike activity and motor behavior indicate that molecular layer interneurons are essential regulators of cerebellar signal coding and memory formation.
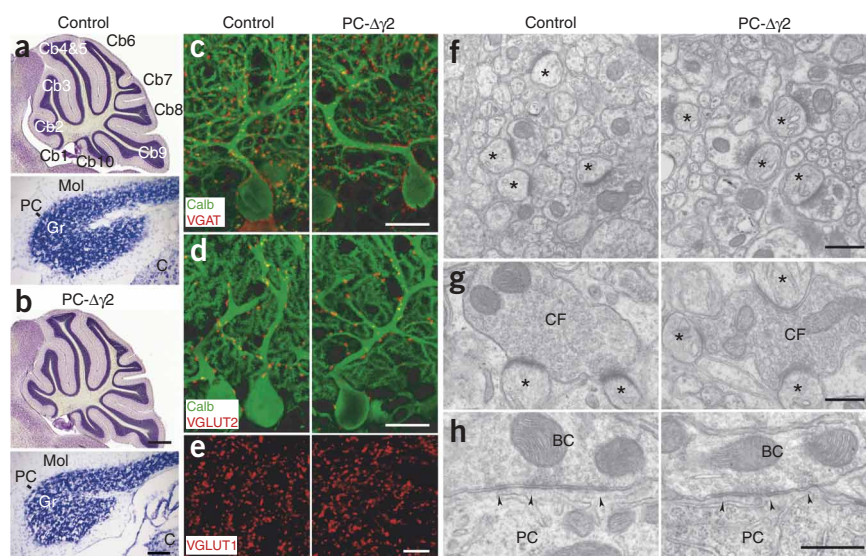
RESULTS

Purkinje cell–specific removal of synaptic GABA$_A$ receptors

To remove GABA$_A$ receptor–mediated feedforward inhibition onto Purkinje cells, we selectively deleted the GABA$_A$ receptor γ2 subunit using the Cre/loxP system (Online Methods). Cre recombinase, under the control of the *L7* promoter, induced a Purkinje cell–specific deletion of the *loxP*-flanked *Gabrg2* (γ2 subunit) gene in the second postnatal week[16,18]. Ablation of synaptic GABA$_A$ receptors from Purkinje cells caused no anatomical alterations of the cerebellar circuitry (**Fig. 1**).

Patch-clamp recordings in acute slices of cerebellar vermis from adult mice showed spontaneous fast inhibitory postsynaptic currents (sIPSCs) at high frequency in all Purkinje cells ($n = 21$) from control mice (**Fig. 2a**), which could be blocked by the GABA$_A$ receptor antagonist SR-95531 (20 μM, data not shown). In contrast, sIPSCs were absent from all Purkinje cells ($n = 19$) of PC-Δγ2 mice (**Fig. 2b**). In some PC-Δγ2 cells (12 of 19), small, slow-rising currents remained. However, these produced on average less than 2% of the control synaptic charge (**Fig. 2**) and probably reflect spillover of synaptically released GABA onto extrasynaptic α and β subunit–containing receptors[19,20] (**Supplementary Fig. 2**). Consistent with a complete loss of synaptic GABA$_A$ receptors, recordings from PC-Δγ2 mice in the presence of tetrodotoxin (TTX) confirmed the absence of miniature IPSCs (mIPSCs; **Fig. 2c,d**). The loss of synaptic GABA$_A$ receptors was

Figure 1 PC-Δγ2 mice show normal cerebellar morphology and synaptic organization. (**a,b**) Nissl stains of sections through vermis (sagittal) and flocculus (coronal) revealed no differences between control (**a**) and PC-Δγ2 (**b**) mice, and the number of Purkinje cells (24.5 ± 2.0 versus 23.9 ± 2.5 cells per 1,000 μm, $P = 0.75$) and molecular layer interneurons (2.36 ± 0.19 versus 2.28 ± 0.18 cells per 1,000 μm², $P = 0.53$) were similar in both groups. C, cochlear nucleus; Cb1–10, lobules 1–10; Gr, granule cell layer; Mol, molecular layer; PC, Purkinje cell layer. (**c–e**) Immunofluorescence labeling in the flocculus showed no differences in the distribution of GABAergic terminals (vesicular γ-aminobutyric acid transporter, VGAT, **c**), climbing fiber terminals (vesicular glutamate transporter 2, VGLUT2, **d**) and parallel fiber terminals (VGLUT1, **e**). Quantification of puncta per 1,000 μm² revealed no difference ($P = 0.27$, 0.62 and 0.68, respectively, $n = 4$). (**f–h**) Electron microscopy showed no obvious morphological changes in parallel and climbing fiber synapses. (**f**) Asymmetric synapses between parallel fibers and Purkinje cell spines (asterisks). The density of parallel fiber to Purkinje cell synapses was unchanged (33.0 versus 32.9 synapses per100 μm² in PC-Δγ2 and control, see Online Methods). (**g**) Asymmetric synapses made by climbing fibers (CF). (**h**) Symmetric synapses (arrowheads) made by basket cells (BC) onto the cell body of Purkinje cells. Scale bars represent 450 μm (**a**) and 150 μm for upper and lower panels, respectively (**b**), 20 μm (**c,d**), 5 μm (**e**), 500 nm (**f**), 360 nm (**g**), and 440 nm (**h**).
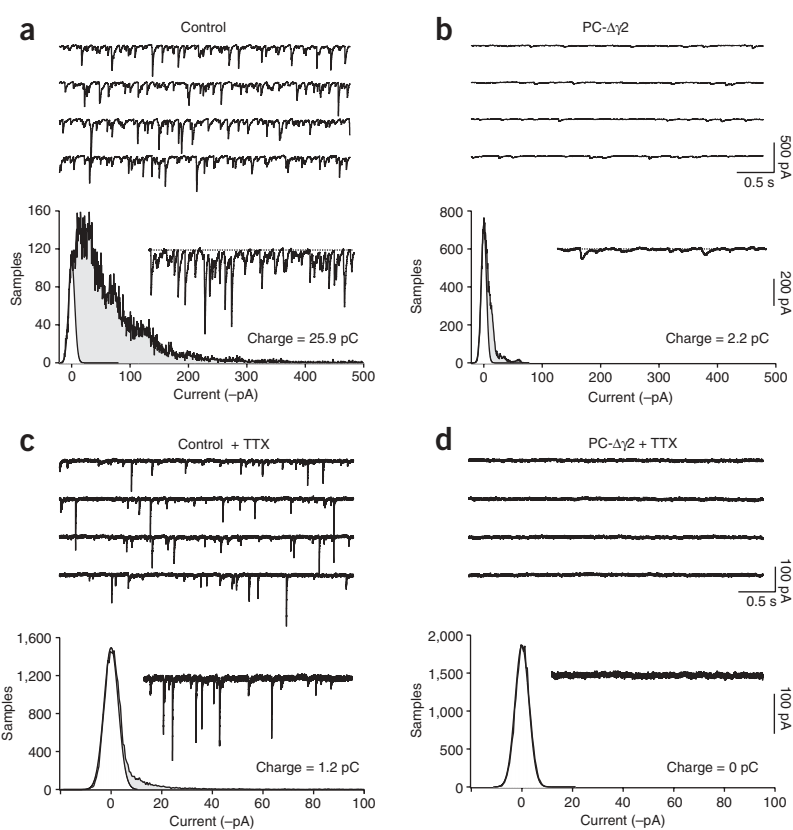
restricted to Purkinje cells; mIPSCs in molecular layer interneurons were unaltered in PC-Δγ2 mice (**Supplementary Fig. 3**).

PC-Δγ2 mice show altered simple spike patterning

Feedforward inhibition via molecular layer interneurons is rapidly (~1 ms) recruited by parallel fiber activation and curtails the parallel fiber–evoked excitatory postsynaptic potential (EPSP) in Purkinje cells[7,21]. To determine how the absence of synaptic GABA$_A$ receptors affected Purkinje cell responses to parallel fiber stimulation, we analyzed the temporal dispersion (jitter) of evoked Purkinje cell simple spikes (**Fig. 3a**). The jitter, quantified as the s.d. of spike latency in a 10-ms window following stimulation (10 V, 100 μs), was strongly

Figure 2 Loss of fast synaptic inhibition from Purkinje cells in PC-Δγ2 mice. (**a**) Representative contiguous segments of a whole-cell recording (–70 mV) from a Purkinje cell of a control mouse. Ionotropic glutamate receptors were blocked with 6-cyano-7-nitroquinoxaline-2,3-dione (CNQX) and D(-)-2-amino-5-phosphonopentanoic acid (D-AP5). Bottom, quantification of mean synaptic charge in a different Purkinje cell, with a 2.5-s recording of sIPSCs and corresponding all-point amplitude histogram. The left-hand peak (most-positive current values), corresponding to the baseline current noise, is fitted with a single-sided Gaussian (white). The peak of the histogram is taken as the zero current value (dotted line in inset). The filled gray area corresponds to all sample points other than those in the baseline noise and thus represents the current produced by phasic synaptic events. In this cell, the mean synaptic charge was 25.9 pC. (**b**) Corresponding data from two PC-Δγ2 mice. sIPSCs were seen in all cells from control mice, but were not observed in cells from PC-Δγ2 mice. Slow SR-95531–sensitive currents were seen in ~60% of PC-Δγ2 cells. For the cell shown in the lower panel, the phasic charge transfer was 2.2 pC. On average, the charge transfer was reduced from 59.8 ± 18.4 pC in control ($n = 8$) to 1.0 ± 0.5 pC in PC-Δγ2 cells ($n = 15$, $P < 0.0002$, Mann-Whitney U test). (**c,d**) Corresponding data recorded in the presence of TTX. Note the different scaling of the current record and the abscissa of the all-point histogram and the complete absence of mIPSCs in PC-Δγ2 cells.

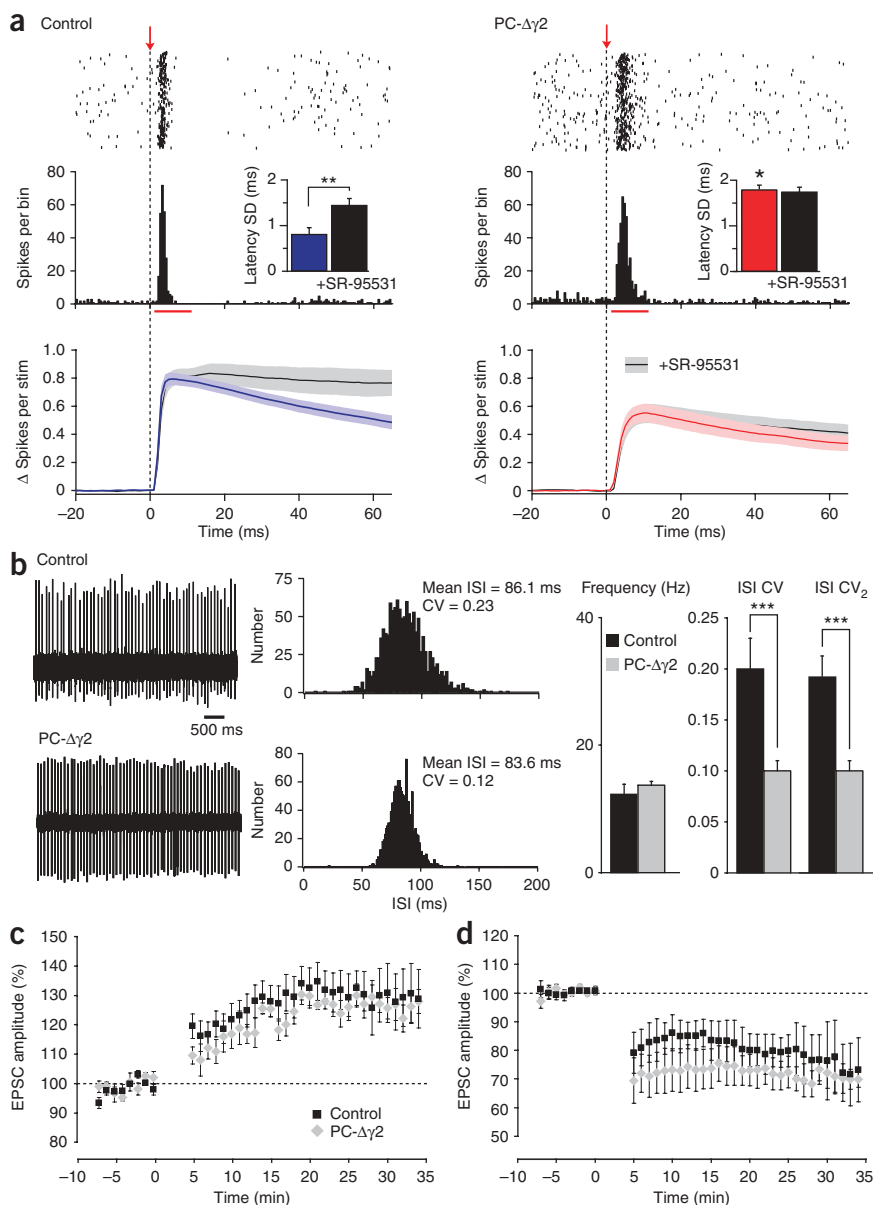**Figure 3** PC-Δγ2 mice show altered parallel fiber–evoked and spontaneous simple-spike firing *in vitro* and unaltered parallel fiber–Purkinje cell LTP and LTD. (**a**) Simple spikes evoked by parallel fiber activation during cell-attached recording. Top and middle panels show raster plots (400 sweeps at 0.5 Hz) and corresponding peristimulus-time histograms (PSTHs, 0.5-ms bin width). Arrows and dashed lines denote stimulation. Insets show s.d. of spike latency in a 10-ms window (red bars, 12 control and 11 PC-Δγ2 cells). Error bars denote s.e.m. Jitter was greater in PC-Δγ2 (red) than in control (blue) cells (*$P < 0.0001$). SR-95531 increased jitter in control cells (**$P = 0.0011$), but not in PC-Δγ2 cells ($P = 0.605$). Bottom, global averages of baseline-corrected cumulative spike probability (see Online Methods). Shaded areas denote s.e.m. (17 control and 13 PC-Δγ2 cells). Stimulation evoked fewer spikes in PC-Δγ2 cells (averaged between 0 and 60 ms, $P = 0.0069$). SR-95531 (40 μM, black line, gray shading) increased spikes in control cells ($n = 11$, $P = 0.0248$), but not in PC-Δγ2 cells ($n = 13$, $P = 0.3199$). (**b**) Representative simple spikes (23–26 °C) and corresponding ISI histograms. Right panels show pooled data (26 control and 9 PC-Δγ2 cells). Although the mean firing rates were not significantly different ($P > 0.05$), the coefficient of variation (CV) and the coefficient of variation of adjacent intervals (CV$_2$) of ISIs differed significantly (***$P < 0.05$) (see text for details). (**c**) Pooled data showing parallel fiber-Purkinje cell LTP in control ($n = 7$, black) and PC-Δγ2 cells ($n = 4$, gray); EPSC amplitude was similarly increased in the strains (both $P < 0.005$; control versus PC-Δγ2, $P = 0.257$). (**d**) Parallel fiber–Purkinje cell LTD was similar in PC-Δγ2 ($n = 5$) and control ($n = 4$) cells (both $P < 0.05$; control versus PC-Δγ2, $P = 0.624$).

increased in PC-Δγ2 Purkinje cells (control, 0.81 ± 0.14 ms, $n = 12$; PC-Δγ2, 1.80 ± 0.10 ms, $n = 11$; $P < 0.0001$). Acute blockade of GABA$_A$ receptors with SR-95531 significantly increased spike jitter in cells from control mice (to 1.45 ± 0.14 ms, $P = 0.0011$; see also ref. 7), but, as expected, had no effect in PC-Δγ2 cells (1.76 ± 0.10 ms, $P = 0.605$). We also determined the number of spikes evoked by parallel fiber stimulation (**Fig. 3a**; see Online Methods). On average, 0.60 ± 0.04 spikes were evoked in the 60 ms following each stimulus in control cells and 0.41 ± 0.05 spikes in PC-Δγ2 cells ($n = 17$ and 13, respectively; $P = 0.0069$). This smaller evoked response is consistent with a reduced parallel fiber excitatory input (see **Supplementary Fig. 4** and Discussion). Consistent with the complete loss of GABA$_A$ receptor–mediated inhibition in PC-Δγ2 cells, SR-95531 increased the number of evoked spikes only in control cells (control, 0.61 ± 0.05 to 0.76 ± 0.08, $n = 11$, $P = 0.0248$; PC-Δγ2, 0.41 ± 0.05 to 0.45 ± 0.06, $n = 13$, $P = 0.3199$). Thus, a loss of molecular layer interneuron–mediated feedforward inhibition in PC-Δγ2 mice results in altered simple-spike responses to parallel fiber inputs.

Purkinje cells in cerebellar slices from PC-Δγ2 mice showed an increase in simple-spike firing regularity compared with controls (**Fig. 3b**). The mean firing rate at 23–26 °C was not different between groups (12.3 ± 1.6 (control) versus 13.7 ± 0.6 Hz (PC-Δγ2), $n = 26$ and 9, $P = 0.062$, Mann-Whitney U test), but the coefficient of variation (s.d. divided by the mean) of the interspike interval (ISI) was reduced in PC-Δγ2 mice (0.20 ± 0.03 in control versus 0.10 ± 0.01 in PC-Δγ2; $P = 0.018$, Mann-Whitney U test). The coefficient of variation of adjacent intervals (mean value of $2 \times \frac{|\mathrm{ISI}_{n+1} - \mathrm{ISI}_n|}{(\mathrm{ISI}_{n+1} + \mathrm{ISI}_n)}$, a measure for the regularity of firing on small timescales[22]) also differed. The coefficient of variation of adjacent intervals was 0.19 ± 0.02 in control versus 0.10 ± 0.01 in PC-Δγ2 mice ($P = 0.018$, Mann-Whitney U test). Blockade of GABA$_A$ receptors with SR-95531 in control Purkinje cells decreased the coefficient of variation of the ISI (0.20 ± 0.04 in control versus 0.13 ± 0.02 in SR-95531 treated, $P = 0.024$, $n = 8$) to a value comparable to that found in PC-Δγ2 mice (see also refs. 12,15,23). As expected, SR-95531 failed to alter the coefficient of variation of the ISI in cells from PC-Δγ2 mice (0.13 ± 0.02 versus 0.13 ± 0.04, $n = 3$). Notably, similar results were obtained at near-physiological temperature (34–35 °C), with no change in the mean rate (51.3 ± 9.1 in control versus 50.0 ± 3.5 Hz in PC-Δγ2, $n = 9$ and 7, $P = 0.61$, Mann-Whitney U test), but a significant decrease in the coefficient of variation (0.14 ± 0.01 in control versus 0.06 ± 0.01 in
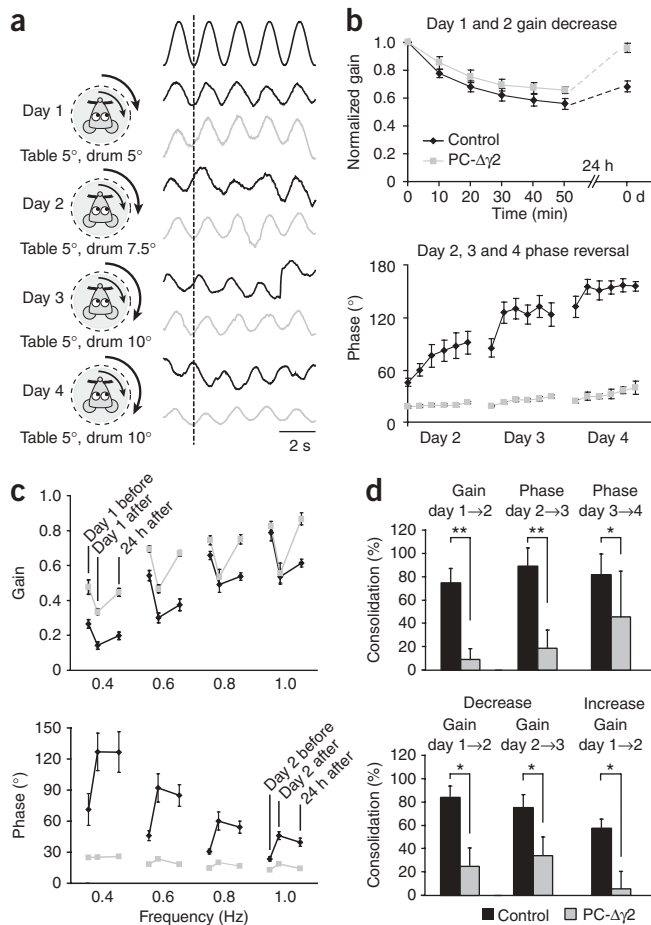
Figure 4 Motor learning is severely affected in PC-Δγ2 mice. (**a**) Illustrations of table and drum rotations (left) during the training procedure and traces (right) of sinusoidal table rotation (top trace) and of VOR eye movements after the training (control, black traces; PC-Δγ2, gray traces). Gain and phase parameters were evaluated five times at 10-min intervals. (**b**) On day 1, PC-Δγ2 and control mice showed similar gain reduction ($P = 0.11$), but the first test on day 2 revealed clear differences ($P = 0.001$) (top). During phase reversal training, control mice learned better than PC-Δγ2 mice (day 4, $P < 0.00001$) (bottom). (**c**) Differences in gain consolidation and phase reversal occurred over a wide range of frequencies. Day 1 before and Day 1 after indicate values before and after training on day 1, and 24 h after indicates the value on the next day, before the next training. (**d**) Top, differences in consolidation (percentage change carried forward from the previous day) for gain decrease (days 1 to 2) and phase reversal (days 2 to 3 and days 3 to 4). Bottom, differences in gain consolidation were also seen with constant in phase drum and table rotation (gain decrease, two histograms on the left) and with constant out of phase drum and table rotation (gain increase, histogram on the right). For the lower panel of **d**, data are from five control and six PC-Δγ2 mice. For all other panels, data are from ten control and nine PC-Δγ2 mice. Error bars denote s.e.m. * $P < 0.05$ and ** $P < 0.01$.

PC-Δγ2, $P = 0.001$; Mann-Whitney U test) and the coefficient of variation of adjacent intervals (0.15 ± 0.02 versus 0.06 ± 0.01, $P = 0.0099$).

Finally, we examined whether a loss of inhibition onto Purkinje cells modified long-term plasticity at parallel fiber to Purkinje cell synapses. Neither parallel fiber long-term depression (LTD) nor long-term potentiation (LTP) (see Online Methods) were significantly impaired in PC-Δγ2 mice compared with controls ($P = 0.624$ and $P = 0.257$, respectively; **Fig. 3c,d**).

Learning and consolidation deficits in PC-Δγ2 mice

PC-Δγ2 mice show no obvious neurological abnormality[16]. To assess cerebellar performance, we analyzed compensatory eye movements in male PC-Δγ2 mice ($n = 9$) and littermate controls ($n = 8$). Mice were exposed to whole-field visual stimuli to determine the amplitude (gain) and timing (phase) of their optokinetic reflex (OKR) and/or tested with turntable stimulation to investigate the same parameters for the vestibulo-ocular reflex in the dark (VOR) and light (visual VOR). PC-Δγ2 mice showed a relatively small, but significant, deficit in their OKR, evident as a reduction in gain and a lag in phase compared with controls ($P = 0.018$ and $P = 0.012$, respectively, two-way repeated-measures ANOVA; **Supplementary Fig. 5**). The VOR gain values and phase leads of PC-Δγ2 mice were larger and smaller, respectively, than those of controls ($P = 0.012$ and $P = 0.030$, two-way repeated-measures ANOVA; **Supplementary Fig. 5**). In contrast, no significant differences were observed during visual VOR ($P = 0.43$ and $P = 0.63$ for gain and phase values, respectively; **Supplementary Fig. 5**). Thus, PC-Δγ2 mice show small, but significant, abnormalities in motor performance when visual and vestibular systems are investigated

separately, but not when they operate together, as under natural conditions or during visuo-vestibular training.

Loss of inhibition onto Purkinje cells had more profound effects on cerebellar motor learning. We studied gain and phase learning by applying a protocol aimed at reducing the gain of the VOR on day 1 (five 10-min sinusoidal, in phase drum and table rotations at 0.6 Hz, both with an amplitude of $5°$) and subsequently shifting its phase on days 2, 3 and 4 (five 10-min sinusoidal, in phase drum and table rotations at 0.6 Hz, but with drum amplitudes of $7.5°$ on day 2 and $10°$ on days 3 and 4, while the table amplitude remained $5°$). Mice were kept in the dark between the recording days.

Gain-decrease learning of PC-Δγ2 ($n = 9$) and control mice ($n = 10$) on day 1 was similar ($P = 0.11$, two-way repeated-measures ANOVA; **Fig. 4a,b**). However, when the measurements were resumed the next day, the degree of gain reduction carried forward from the previous day's learning was significantly smaller in PC-Δγ2 mice than in controls ($P = 0.001$; **Fig. 4b**). This consolidation deficit was apparent at a wide range of frequencies (**Fig. 4c**). To exclude nonspecific effects (habituation during gain-decrease learning), we tested PC-Δγ2 and control mice in nonadapting VOR protocols; notably, mice of both genotypes showed no significant decreases in VOR over consecutive days (last gain value of session 1 versus first value of session 2, $P = 0.610$ for controls and 0.551 for PC-Δγ2 mice; **Supplementary Fig. 6**).

Deficits in gain consolidation were also seen when the drum rotation amplitude was kept constant (three 10-min sinusoidal, in phase drum and table rotations at 0.6 Hz, both with an amplitude of $5°$; **Fig. 4d**). Here too, the initial level of learning was not significantly affected (PC-Δγ2 mice versus controls, $P = 0.61$; $n = 6$ and 5, respectively), whereas the level of consolidation was significantly reduced (gain day 1 → 2, $P = 0.034$; gain day 2 → 3, $P = 0.046$). Moreover, gain consolidation deficits in PC-Δγ2 mice did not depend on the direction of learning. With a gain-increase protocol (five 10-min sinusoidal, out of phase drum and table rotation at 1.0 Hz, both with an amplitude of $1.6°$), no significant consolidation was present in the PC-Δγ2 mice (gain day 1 → 2, $P = 0.744$, $n = 6$, one-Sample t test). In contrast, consolidation in control mice was present and was significantly stronger than in PC-Δγ2 mice ($P = 0.002$; **Fig. 4d**). Notably, the level of gain-increase learning in PC-Δγ2 mice was not significantly different from that in controls ($P = 0.800$). Thus, deficits in consolidation of learned gain changes during both gain-decrease and gain-increase training procedures were not the results of differences in baseline performance.
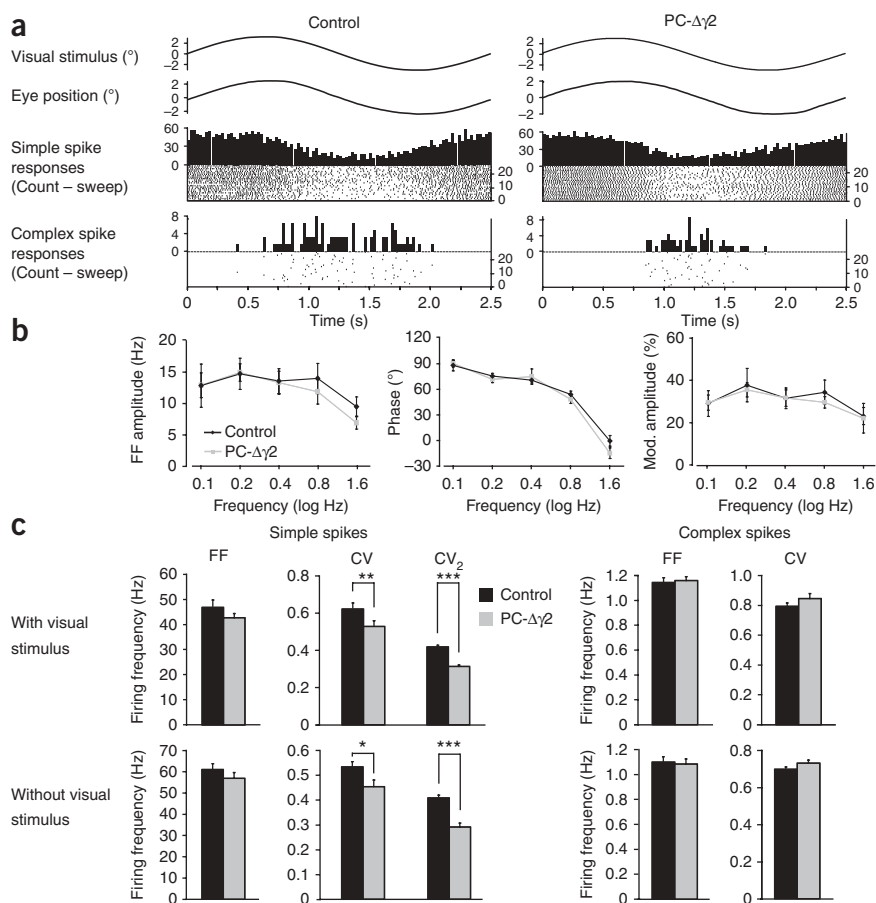
Figure 5 Temporal patterns of simple spike activities of floccular Purkinje cells are specifically affected in PC-Δγ2 mice during both compensatory eye movement behavior and spontaneous behavior. (**a**) Representative single-unit activity recorded from Purkinje cells in the flocculus of a control and a PC-Δγ2 mouse during fixed velocity (8° s^{-1}, 0.2 Hz) OKR stimulation. The visual stimulus and eye position are shown together with histograms of simple spike and complex spike frequencies and corresponding raster plots. Count (frequency) is the number of spikes per bin divided by bin size, and sweep is the cycle number. (**b**) Firing frequency (FF) amplitude, phase relative to stimulus and amplitude of modulation (see Online Methods) of floccular simple-spike activities during optokinetic stimulation (8° s^{-1}, 0.1–1.6 Hz) were not significantly different between PC-Δγ2 and control mice ($P > 0.3$). (**c**) Although the average firing frequency of simple and complex spike activity did not differ between PC-Δγ2 and control mice, the coefficient of variation of simple spikes in PC-Δγ2 mice was significantly reduced in recordings both with and without visual stimuli ($P = 0.008$ and $P = 0.022$, respectively). Also, the coefficient of variation of adjacent intervals values of simple spikes were significantly lower than those of controls in both conditions. Error bars denote s.e.m. * $P < 0.05$, ** $P < 0.01$ and *** $P < 0.0001$.

The adaptation procedure provided on days 2, 3 and 4 immediately revealed significant deficits in phase learning in PC-Δγ2 mice, starting 10–20 min after the initiation of visuo-vestibular training (for example, at 20 min, $P = 0.009$; **Fig. 4b**). These deficits in phase change acquisition were followed by clear differences in consolidation (for example, from day 2 to day 3, $P = 0.0008$; **Fig. 4d**). Phase adaptation deficits also occurred at a wide range of frequencies (**Fig. 4c**) and were not caused by visual problems in PC-Δγ2 mice, as eye movement recordings during the adaptation sessions showed that PC-Δγ2 mice were capable of full phase reversal (**Supplementary Fig. 7**). In short, PC-Δγ2 mice showed a relatively normal capacity for acquisition during gain-decrease and gain-increase motor learning, but a profound deficit in acquisition during phase adaptation learning and a general deficit in consolidation of gain and phase adaptation.

Abnormal temporal patterns of Purkinje cell simple spikes

Because the flocculus controls the adaptation of compensatory eye movements[24–26] and Purkinje cells provide the sole output of the cerebellar cortex (**Supplementary Fig. 1**), we analyzed floccular Purkinje cell activity during optokinetic stimulation (**Fig. 5a**). Single units of Purkinje cells that responded optimally to stimulation around the vertical axis were identified by creating tuning curves of their complex spike responses and by identifying a clean climbing fiber pause[26,27]. The average climbing fiber pause in PC-Δγ2 mice and controls was 15.3 ± 0.8 and 18.6 ± 1.3 ms, respectively (55 and 60 PC-Δγ2 and control cells, respectively, $P = 0.029$). The average simple-spike firing frequency amplitude, phase relative to stimulus and modulation amplitude were similar in PC-Δγ2 and control mice (**Fig. 5b**). However, as predicted by our *in vitro* recordings, the regularity of Purkinje cell firing was affected.

For floccular simple-spike activities, the coefficient of variation of the ISIs was significantly reduced during visual stimulation in PC-Δγ2 mice ($P = 0.008$; PC-Δγ2, $n = 55$; controls, $n = 60$; **Fig. 5c**). This difference reflected specific changes in temporal patterning, as the coefficient of variation of adjacent intervals was significantly lower in PC-Δγ2 mice ($P < 0.0001$; **Fig. 5c**, see also **Supplementary Fig. 8**).
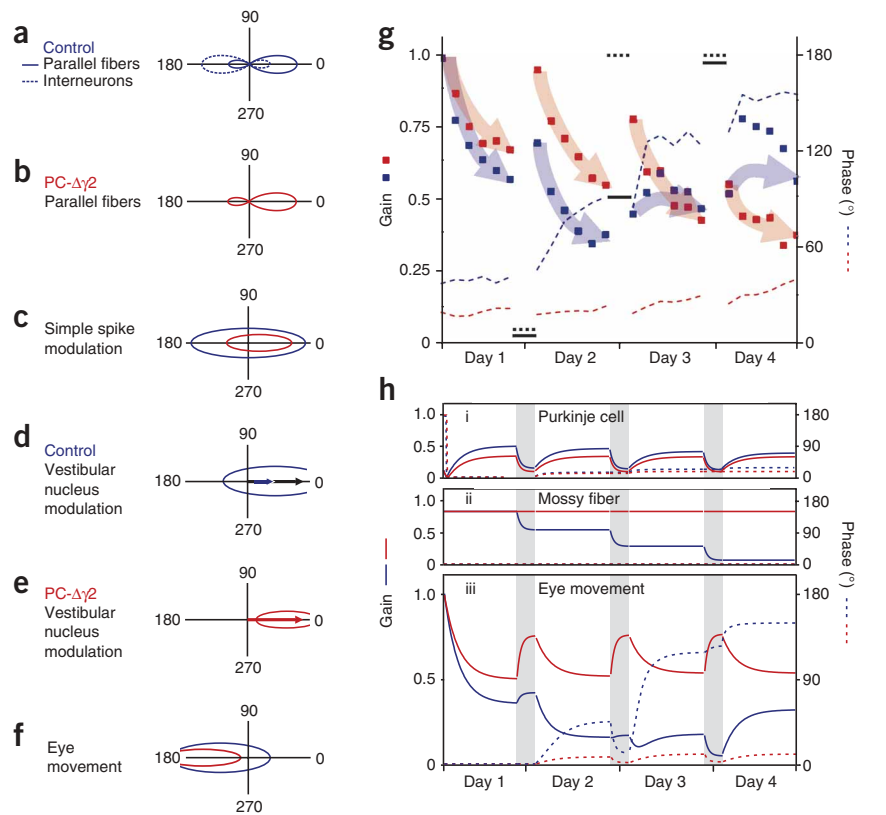
If differences in Purkinje cell firing patterns contribute to consolidation deficits in PC-Δγ2 mice, we would also expect to find them outside of periods of optokinetic stimulation. Indeed, both the coefficient of variation and the coefficient of variation of adjacent intervals of ISIs were significantly reduced in the absence of stimulation ($P = 0.022$ and $P < 0.0001$, respectively; PC-Δγ2, $n = 41$; controls, $n = 43$; **Fig. 5c**). In contrast, the patterns of complex spike activities of Purkinje cells did not differ between PC-Δγ2 and control mice (**Fig. 5a,c**, see also **Supplementary Fig. 9**). Also, the antiphasic modulation of complex and simple spikes was unchanged (**Fig. 5a**), arguing against a critical involvement of molecular layer interneurons in this phenomenon[8].

Model and simulations

We interpreted the experimental data from the 4-d gain-decrease, phase adaptation routine using a 'distributed memory' model (**Fig. 6**). Short-term adaptation is assumed to take place in the cerebellar cortex and is expressed as adaptation of the phase and gain of modulation of Purkinje cell simple spikes, which in turn modulate the activity of target neurons in the vestibular nucleus; this process underlies the rapid VOR gain adaptation observed in both PC-Δγ2 and control mice. On a longer timescale, the learned Purkinje cell activity guides plasticity at the target neurons in the vestibular nuclei[28,29], the polarity of which is presumably regulated by the precise timing of simple spikes relative to input from mossy fiber collaterals[30]. Simultaneously, a partial extinction of the previously learned changes at the level of the Purkinje cells takes

Figure 6 Interpretation of VOR adaptation data using a distributed memory model. (**a**) Modeled activation of parallel fibers and interneurons plotted in polar coordinates. Most parallel fibers modulate (increase activation) in phase with ipsilateral head movement (0°), whereas a fraction responds to input from the contralateral horizontal canal (180°). Interneurons are modeled similarly, but with an opposite sign representing their inhibitory nature. (**b**) Data are presented as in **a**, but for PC-Δγ2 mice lacking inhibition. (**c**) Maximum simple-spike modulation attainable by appropriate depression and potentiation of the excitatory and inhibitory inputs shown in **a** and **b** for control (blue) and PC-Δγ2 (red) mice (based on linear input summation). (**d**) Modulation of target vestibular nucleus neurons attainable by linear summation of mossy fiber inputs (blue arrow, in phase with head movement) and Purkinje cell inputs (**c**, blue curve) in control mice. The black arrow represents the efficacy of mossy fiber input before training. (**e**) Data are presented as in **d**, but for PC-Δγ2 mice, where the efficacy of plasticity at the mossy fiber synapses is presumably impaired. (**f**) Limited simple-spike modulation and mossy fiber plasticity restrained eye movements in PC-Δγ2 mice (red) compared with control mice (blue). The control curve also covers the area of VOR phase reversal, from out-of-phase with head movement (180° in this figure) to in-phase (0°). (**g**) Experimental data; squares represent VOR gain and dashed lines represent VOR phase relative to the head (shifted by 180°, for ease of illustration; see also **Fig. 4**). For each session, after initial adaptation, the learned Purkinje cell signal determines the new 'desired' phase and gain state for the vestibular nucleus neurons (dashed and solid black bars, respectively). The superimposed blue (control) and red (PC-Δγ2) arrows indicate the direction of change. (**h**) Simulation of the training procedure shown in **g**. During training, Purkinje cells rapidly approached their target modulation (i), reflecting short-term VOR adaptation. Purkinje cell–guided plasticity of mossy fiber input to vestibular nuclei (ii) allowed control mice to gradually adapt the phase of their VOR during prolonged training (iii). In PC-Δγ2 mice, loss of vestibular nucleus consolidation impaired phase adaptation. For simplicity, adaptation in the vestibular nuclei and partial extinction of cortical memory were simulated to occur between training sessions (gray bars).

place[31]. The memory is thus partially transferred to the target nuclei, potentially underlying long-term consolidation[29,32]. After several days of training, this form of 'systems consolidation' ensures that the cerebellar cortex is no longer responsible for the expression of the learned behavior, but mainly regulates the precise timing (phase). In PC-Δγ2 mice, the altered temporal patterns of Purkinje cell simple spikes could impair the induction of plasticity in the nuclei and thus consolidation.

Given this working hypothesis, we examined whether deficits in VOR gain consolidation and phase adaptation in PC-Δγ2 mice could be replicated in a conceptual model of the idealized VOR circuit (**Supplementary Data**). We modeled the modulation of Purkinje cell simple-spike firing during head movement resulting from linear summation of sinusoidal excitatory (parallel fiber) and inhibitory (interneuron) inputs[6] (**Fig. 6a,b**). We assumed the gain and phase of such modulation to be regulated through bidirectional plasticity of the inputs[33] (**Fig. 6c**) and that Purkinje cells and mossy fiber collaterals subsequently modulate, by linear summation of their activity, the firing of cells in the vestibular nuclei (**Fig. 6d,e**), which in turn control eye movement (**Fig. 6f**). As a result of the absence of inhibition in PC-Δγ2 mice, the simple spike activation required for adequate modulation of the vestibular nucleus was out of range of the normal plasticity mechanisms in the cerebellar cortex (**Fig. 6c**). In addition, impaired plasticity of the inputs to the vestibular nucleus (**Fig. 6e**) both abolished consolidation and excluded the possibility of extreme phase adaptations (**Fig. 6f**).

Data from four training sessions, each followed by an overnight period (**Fig. 6g**), were simulated using the upper bounds on sinusoidal modulation (**Fig. 6a–f**). Adaptation of modulation (**Fig. 6h**) was simulated as an exponential decay from the start position in the polar plot (defined by the initial gain and phase) toward a new position determined by the experimental procedure (**Fig. 6g**). Simulation parameters were chosen to mimic the rate of adaptation observed experimentally (**Supplementary Data**). Under these conditions, both control and PC-Δγ2 Purkinje cells rapidly reached the required modulation during short-term VOR adaptation (**Fig. 6h**). However, impairments in both VOR gain consolidation and phase adaptation can be generated if we assume that disrupted plasticity in the vestibular nucleus is caused by poor timing of simple spikes (**Figs. 3**, **5** and **6h**).

DISCUSSION
Signal coding and plasticity in cerebellar learning
Although inhibitory interneurons in the molecular layer of the cerebellum have been studied extensively[5–8], their behavioral relevance has remained enigmatic. We found that these interneurons shape the temporal patterns of Purkinje cell simple spikes and suggest that this process could be essential for plasticity and consolidation in the cerebellar and vestibular nuclei.

Floccular Purkinje cells control the adaptation of compensatory eye movements by modulating the activity of vestibular nucleus neurons (**Supplementary Fig. 1**). To adapt the VOR, two things should happen in the framework of a distributed memory model. First, Purkinje cells

should 'learn' the correct simple-spike modulation and express it at sufficient gain to modulate the vestibular nuclei. Second, the input from the direct vestibular pathway to the vestibular nuclei should be suppressed, as it only allows modulation in phase with ipsilateral head movement. The first of these processes is thought to reflect complementary inhibitory and excitatory actions, with plasticity at parallel fiber to Purkinje cell and parallel fiber to interneuron synapses, both under climbing fiber control[13,24,25]. The second is thought to occur through plasticity at mossy fiber to vestibular nuclei synapses[25,28]. In PC-Δγ2 mice, the temporal fidelity of Purkinje cell firing was disrupted and consolidation of learned VOR adaptations was severely compromised (**Figs. 4** and **6g**). As induction of various forms of plasticity in the vestibular and cerebellar nuclei could depend on the precise timing of inhibitory and excitatory input from Purkinje cells and mossy fiber collaterals (**Supplementary Data**), disruption of this timing would impair transfer of plasticity to the nuclei and thus impair systems consolidation.

Simple spike trains in Purkinje cells show substantially more temporal patterns than expected from random activation and these patterns are influenced by natural stimuli[22]. Both the electrical coupling among interneurons and the sagittal orientation of their axons[34,35] (**Supplementary Fig. 1**) could enhance the effects of feedforward inhibition by promoting common firing patterns in ensembles of Purkinje cells in individual zones that are known to project to the same nucleus[26]. The activity patterns of individual Purkinje cells in an ensemble might thus interact with each other and/or with those of mossy fiber and/or climbing fiber collaterals to facilitate the induction of plasticity in the cerebellar and vestibular nuclei[25,28,36,37]. We therefore propose that the vestibular nuclei are the locus for consolidation (see also refs. 29,32). Alternatively, both initial learning and consolidation could occur in the cerebellar cortex and the consolidation signal could be preserved in the average simple-spike frequency of a particular Purkinje cell. In fact, changes in simple-spike frequencies in the flocculus of monkeys are sufficient to drive changes in eye velocity during trial-by-trial motor learning[38]. To determine the extent to which spatiotemporal patterns of simple spikes contribute to consolidation and whether this consolidation occurs in the nuclei, future experiments will require simultaneous multi-unit recording from ensembles of Purkinje cells and cerebellar or vestibular nuclei neurons during learning.

Previous studies have identified long-term changes at the parallel fiber to Purkinje cell synapse as a potential plasticity mechanism during cerebellar learning, and some mouse lines with disrupted LTD induction at this synapse show impaired motor learning[39–41]. However, neither parallel fiber LTD nor LTP were impaired in PC-Δγ2 mice. Notably, the motor learning deficits in PC-Δγ2 mice differed from those seen in mouse lines in which LTD was impaired by blocking PKC, PKG or αCaMKII activity in Purkinje cells. Furthermore, in the latter mouse lines, acute learning was affected more severely than in PC-Δγ2 mice, whereas learning over multiple days of training was less affected[39–42].

GABAergic interneurons in the cerebellar cortex have ample possibilities to induce and express plasticity at both the synaptic input and output level[1,9,13,43–45]. Simultaneous induction of LTP at molecular layer interneuron and parallel fiber to Purkinje cell synapses is required for associative fear conditioning[9]. In this scenario, the potentiation of GABAergic synapses may balance the LTP of excitatory inputs in a form of scaling to preserve coincidence detection of parallel fiber inputs[7,9], which mirrors the balanced LTD seen at parallel fiber and interneuron synapses with the same conjunctive climbing fiber pairing[45]. Loss of this scaling mechanism in PC-Δγ2 mice might contribute to the observed phenotype.

Inhibition is essential for spike patterning and learning

Although PC-Δγ2 mice showed marked deficits in cerebellar motor learning, baseline motor performance was only moderately affected. Despite the lack of synaptic GABA_A receptors on PC-Δγ2 Purkinje cells, we found their average simple-spike frequency to be normal. This could reflect enhancement of another inhibitory input (for example, GABA_B receptors) and/or reduced parallel fiber excitatory input. Although GABA_B receptor–mediated inhibition of PC-Δγ2 Purkinje cells was unchanged (**Supplementary Fig. 10**), we found a significant decrease in AMPA receptor–mediated EPSC charge transfer after parallel fiber stimulation ($P < 0.0025$; **Supplementary Fig. 4**). This might allow Purkinje cells to maintain their excitability in a normal operational range in the absence of fast inhibition. In contrast, the loss of temporal fidelity in Purkinje cell responses to parallel fiber stimulation and the increase in simple-spike regularity in PC-Δγ2 mice were comparable to the changes seen after acute pharmacological blockade of GABA_A receptors[7,12] (**Figs. 3** and **5**). The cerebellum may thus compensate for the loss of certain functions of molecular layer interneurons, but these interneurons are essential for the temporal control of Purkinje cell activity and for both phase adaptation learning and consolidation of gain adaptations.

By deleting synaptic GABA_A receptors from Purkinje cells in PC-Δγ2 mice, we also disrupted any inhibition mediated by recurrent collaterals of Purkinje cell axons[10,46]. However, because GABAergic terminals from basket and stellate cells onto Purkinje cells vastly outnumber those from recurrent collaterals and because Purkinje-Purkinje contacts in mice tend to be restricted to young animals[46], the phenotype that we observed is most likely caused by the loss of inhibition from molecular layer interneurons. Moreover, although it has been proposed that Purkinje cell axon collaterals contribute to fast cerebellar oscillations in adult rats[47], such oscillations have not been recorded in wild-type mice[10].

General functional implications

Studies on learning and memory have focused largely on the role of plasticity at excitatory synapses onto projecting neurons. However, GABAergic interneurons also express plasticity, which increases the computational capacity of their microcircuit[1,2,9]. We examined the role of fast synaptic inhibition in cerebellar motor learning using genetic dissection of the circuit and our results suggest that feedforward inhibition is essential for specific aspects of procedural learning.

Can our findings be extrapolated to other brain regions? Feedforward inhibition is a common motif throughout the CNS. In the amygdala, it mediates extinction learning of conditioned fear responses[48]. In cortical circuits, some interneuron types may serve functions similar to those that we identified in the cerebellum. For example, feedforward inhibitory interneurons in the hippocampus may promote the temporal fidelity of synaptic integration and action potential generation in pyramidal cells necessary for encoding declarative memories[2,3]. Thus, feedforward inhibition might be an operational necessity for memory formation in different brain circuits.

METHODS

Methods and any associated references are available in the online version of the paper at http://www.nature.com/natureneuroscience/.

Note: Supplementary information is available on the Nature Neuroscience website.

1. Smith, S.L. & Otis, T.S. Pattern-dependent, simultaneous plasticity differentially transforms the input-output relationship of a feedforward circuit. *Proc. Natl. Acad. Sci. USA* **102**, 14901–14906 (2005).
2. Kullmann, D.M. & Lamsa, K.P. Long-term synaptic plasticity in hippocampal interneurons. *Nat. Rev. Neurosci.* **8**, 687–699 (2007).
3. Pouille, F. & Scanziani, M. Enforcement of temporal fidelity in pyramidal cells by somatic feed-forward inhibition. *Science* **293**, 1159–1163 (2001).
4. Lamsa, K., Heeroma, J.H. & Kullmann, D.M. Hebbian LTP in feed-forward inhibitory interneurons and the temporal fidelity of input discrimination. *Nat. Neurosci.* **8**, 916–924 (2005).
5. Eccles, J.C., Ito, M. & Szentagothai, J. *The Cerebellum as a Neuronal Machine* (Springer-Verlag, New York, 1967).
6. Miyashita, Y. & Nagao, S. Contribution of cerebellar intracortical inhibition to Purkinje cell response during vestibulo-ocular reflex of alert rabbits. *J. Physiol. (Lond.)* **351**, 251–262 (1984).
7. Mittmann, W., Koch, U. & Hausser, M. Feed-forward inhibition shapes the spike output of cerebellar Purkinje cells. *J. Physiol. (Lond.)* **563**, 369–378 (2005).
8. Barmack, N.H. & Yakhnitsa, V. Functions of interneurons in mouse cerebellum. *J. Neurosci.* **28**, 1140–1152 (2008).
9. Scelfo, B., Sacchetti, B. & Strata, P. Learning-related long-term potentiation of inhibitory synapses in the cerebellar cortex. *Proc. Natl. Acad. Sci. USA* **105**, 769–774 (2008).
10. Orduz, D. & Llano, I. Recurrent axon collaterals underlie facilitating synapses between cerebellar Purkinje cells. *Proc. Natl. Acad. Sci. USA* **104**, 17831–17836 (2007).
11. Davie, J.T., Clark, B.A. & Hausser, M. The origin of the complex spike in cerebellar Purkinje cells. *J. Neurosci.* **28**, 7599–7609 (2008).
12. Häusser, M. & Clark, B.A. Tonic synaptic inhibition modulates neuronal output pattern and spatiotemporal synaptic integration. *Neuron* **19**, 665–678 (1997).
13. Jörntell, H. & Ekerot, C.F. Reciprocal bidirectional plasticity of parallel fiber receptive fields in cerebellar Purkinje cells and their afferent interneurons. *Neuron* **34**, 797–806 (2002).
14. Santamaria, F., Tripp, P.G. & Bower, J.M. Feedforward inhibition controls the spread of granule cell–induced Purkinje cell activity in the cerebellar cortex. *J. Neurophysiol.* **97**, 248–263 (2007).
15. Raman, I.M. & Bean, B.P. Resurgent sodium current and action potential formation in dissociated cerebellar Purkinje neurons. *J. Neurosci.* **17**, 4517–4526 (1997).
16. Wulff, P. *et al.* From synapse to behavior: rapid modulation of defined neuronal types with engineered GABA$_A$ receptors. *Nat. Neurosci.* **10**, 923–929 (2007).
17. Schweizer, C. *et al.* The gamma 2 subunit of GABA(A) receptors is required for maintenance of receptors at mature synapses. *Mol. Cell. Neurosci.* **24**, 442–450 (2003).
18. Barski, J.J., Dethleffsen, K. & Meyer, M. Cre recombinase expression in cerebellar Purkinje cells. *Genesis* **28**, 93–98 (2000).
19. Brickley, S.G., Cull-Candy, S.G. & Farrant, M. Single-channel properties of synaptic and extrasynaptic GABA$_A$ receptors suggest differential targeting of receptor subtypes. *J. Neurosci.* **19**, 2960–2973 (1999).
20. Lorez, M., Benke, D., Luscher, B., Mohler, H. & Benson, J.A. Single-channel properties of neuronal GABA$_A$ receptors from mice lacking the gamma2 subunit. *J. Physiol. (Lond.)* **527**, 11–31 (2000).
21. Brunel, N., Hakim, V., Isope, P., Nadal, J.P. & Barbour, B. Optimal information storage and the distribution of synaptic weights: perceptron versus Purkinje cell. *Neuron* **43**, 745–757 (2004).
22. Shin, S.L. *et al.* Regular patterns in cerebellar Purkinje cell simple spike trains. *PLoS One* **2**, e485 (2007).
23. Walter, J.T., Alvina, K., Womack, M.D., Chevez, C. & Khodakhah, K. Decreases in the precision of Purkinje cell pacemaking cause cerebellar dysfunction and ataxia. *Nat. Neurosci.* **9**, 389–397 (2006).
24. Ito, M. Cerebellar flocculus hypothesis. *Nature* **363**, 24–25 (1993).
25. Lisberger, S.G. Cerebellar LTD: a molecular mechanism of behavioral learning? *Cell* **92**, 701–704 (1998).
26. Schonewille, M. *et al.* Zonal organization of the mouse flocculus: physiology, input and output. *J. Comp. Neurol.* **497**, 670–682 (2006).
27. Hoebeek, F.E. *et al.* Increased noise level of Purkinje cell activities minimizes impact of their modulation during sensorimotor control. *Neuron* **45**, 953–965 (2005).
28. Gittis, A.H. & du Lac, S. Intrinsic and synaptic plasticity in the vestibular system. *Curr. Opin. Neurobiol.* **16**, 385–390 (2006).
29. Kassardjian, C.D. *et al.* The site of a motor memory shifts with consolidation. *J. Neurosci.* **25**, 7979–7985 (2005).
30. Medina, J.F. & Mauk, M.D. Computer simulation of cerebellar information processing. *Nat. Neurosci.* **3** Suppl: 1205–1211 (2000).
31. Medina, J.F., Nores, W.L. & Mauk, M.D. Inhibition of climbing fibers is a signal for the extinction of conditioned eyelid responses. *Nature* **416**, 330–333 (2002).
32. Shutoh, F., Ohki, M., Kitazawa, H., Itohara, S. & Nagao, S. Memory trace of motor learning shifts transsynaptically from cerebellar cortex to nuclei for consolidation. *Neuroscience* **139**, 767–777 (2006).
33. Coesmans, M., Weber, J.T., De Zeeuw, C.I. & Hansel, C. Bidirectional parallel fiber plasticity in the cerebellum under climbing fiber control. *Neuron* **44**, 691–700 (2004).
34. Mann-Metzer, P. & Yarom, Y. Electrotonic coupling interacts with intrinsic properties to generate synchronized activity in cerebellar networks of inhibitory interneurons. *J. Neurosci.* **19**, 3298–3306 (1999).
35. Van Der Giessen, R.S., Maxeiner, S., French, P.J., Willecke, K. & De Zeeuw, C.I. Spatiotemporal distribution of Connexin45 in the olivocerebellar system. *J. Comp. Neurol.* **495**, 173–184 (2006).
36. Steuber, V. *et al.* Cerebellar LTD and pattern recognition by Purkinje cells. *Neuron* **54**, 121–136 (2007).
37. Blazquez, P.M., Hirata, Y. & Highstein, S.M. Chronic changes in inputs to dorsal Y neurons accompany VOR motor learning. *J. Neurophysiol.* **95**, 1812–1825 (2006).
38. Medina, J.F. & Lisberger, S.G. Links from complex spikes to local plasticity and motor learning in the cerebellum of awake-behaving monkeys. *Nat. Neurosci.* **11**, 1185–1192 (2008).
39. De Zeeuw, C.I. *et al.* Expression of a protein kinase C inhibitor in Purkinje cells blocks cerebellar LTD and adaptation of the vestibulo-ocular reflex. *Neuron* **20**, 495–508 (1998).
40. Feil, R. *et al.* Impairment of LTD and cerebellar learning by Purkinje cell–specific ablation of cGMP-dependent protein kinase I. *J. Cell Biol.* **163**, 295–302 (2003).
41. Hansel, C. *et al.* alphaCaMKII Is essential for cerebellar LTD and motor learning. *Neuron* **51**, 835–843 (2006).
42. Boyden, E.S. *et al.* Selective engagement of plasticity mechanisms for motor memory storage. *Neuron* **51**, 823–834 (2006).
43. Kano, M., Rexhausen, U., Dreessen, J. & Konnerth, A. Synaptic excitation produces a long-lasting rebound potentiation of inhibitory synaptic signals in cerebellar Purkinje cells. *Nature* **356**, 601–604 (1992).
44. Duguid, I.C. & Smart, T.G. Retrograde activation of presynaptic NMDA receptors enhances GABA release at cerebellar interneuron–Purkinje cell synapses. *Nat. Neurosci.* **7**, 525–533 (2004).
45. Mittmann, W. & Hausser, M. Linking synaptic plasticity and spike output at excitatory and inhibitory synapses onto cerebellar Purkinje cells. *J. Neurosci.* **27**, 5559–5570 (2007).
46. Watt, A.J. *et al.* Traveling waves in developing cerebellar cortex mediated by asymmetrical Purkinje cell connectivity. *Nat. Neurosci.* **12**, 463–473 (2009).
47. de Solages, C. *et al.* High-frequency organization and synchrony of activity in the Purkinje cell layer of the cerebellum. *Neuron* **58**, 775–788 (2008).
48. Likhtik, E., Popa, D., Apergis-Schoute, J., Fidacaro, G.A. & Pare, D. Amygdala intercalated neurons are required for expression of fear extinction. *Nature* **454**, 642–645 (2008).

ONLINE METHODS

Procedures involving mice were performed in accordance with regulations of the United Kingdom Animals (Scientific Procedures) Act 1986, the Animal Care and Use Committee of Turin University and the Dutch Ethical Committee for animal experiments.

Generation of PC-Δγ2 mice. We generated *γ2I77lox* mice by flanking exon 4 of the *Gabrg2* gene with *loxP* sites and changing the codon encoding F77 in exon 4 to I, which resulted in a neutral amino acid substitution[16]. Homozygous *γ2I77lox* mice were crossed with mice heterozygous for *γ2I77lox* and hemizygous for an *L7-cre* transgene[16,18]. *γ2I77lox/γ2I77lox; L7-cre* (PC-Δγ2) and *γ2I77lox/γ2I77lox* (controls) littermates were used. Mice were genotyped by PCR analysis of genomic DNA using primers to test for the *γ2I77lox* allele (213-bp control, 250-bp *γ2I77lox*) (γ2lx5′_s (5′-GTCATGCTAAATATCCTA CAGTGG-3′) and γ2lx5′_as (5′-GGATAGTGCATCAGCAGACAATAG-3′)) and primers to test for the *cre* transgene (250-bp *L7Cre*) (Cre1 (5′-GAC CAGGTTCGTTCACTCATGG-3′) and Cre2 (5′-AGGCTAAGTGCCTTCTCTA CAC-3′)).

Morphology. Adult mice were anaesthetized by intraperitoneal injection of ketamine/xylazine and perfused with 4% paraformaldehyde (wt/vol) in phosphate-buffered saline (PBS, pH7.4). Cerebella were cryoprotected in sucrose (10%, 20% and 30% in PBS, wt/vol) and cut into 16-μm coronal sections with a cryostat. Following blocking in normal goat serum (10% in PBS, vol/vol with 0.5% Triton X-100, vol/vol), sections were incubated with antibodies to calbindin (1:10,000, Swant), VGAT (1:3,000), VGLUT1 (1:1,000) or VGLUT2 (1:500, all Synaptic Systems). Sections were rinsed and incubated with secondary antibodies conjugated to Alexa 488 (Molecular Probes) or Cy3 (Jackson Immunoresearch). Sections were examined with a laser-scanning confocal microscope (Zeiss LSM5 Pascal). Stacks of 5–15 sections spaced 250–350 nm apart were acquired (pinhole, 1 Airy unit). Quantification of VGLUT2-positive puncta was carried out on segmented images spanning the molecular layer; eight confocal fields (13,225 μm^2 per field) were counted per mouse ($n = 4$). For VGLUT1 and VGAT, images acquired at a magnification of 8.1×10^{-3} μm^2 per pixel (512 × 512 pixels) were segmented using a threshold that maximized the selection of immunofluorescent puncta over background. The number and density of puncta were calculated with ImageJ software (http://rsbweb.nih.gov/ij/). For VGLUT1 and VGAT, six and eight fields (2,125 μm^2 per field) were counted per mouse ($n = 3$ and 4, respectively). To quantify the number of Purkinje cells, we placed a line through the Purkinje cell layer and counted all of the calbindin-positive cells on the line (four sections per mouse, $n = 4$). The density of molecular layer interneurons was calculated in 3–6 fields (5,000 μm^2 per field) of 3–5 Nissl-stained sections per mouse ($n = 4$).

For electron microscopy, adult mice ($n = 2$ per genotype) were perfused with 4% paraformaldehyde and 2.5% glutaraldehyde (vol/vol) in phosphate buffer (0.1 M, pH 7.4). Cerebella were postfixed in the same solution overnight. Blocks of tissue were postfixed in 1% osmium tetroxide (vol/vol, in 0.1 M cacodylate buffer), dehydrated in ethanol and embedded in Epon-Araldite. Ultrathin sections were stained with uranyl acetate and lead citrate and analyzed with a JEM-1010 transmission electron microscope (Jeol) equipped with a side-mounted CCD camera (Mega View III, Soft Imaging System). In each mouse, 90 electron micrographs were taken randomly from the neuropil of the molecular layer at a magnification of 30,000× (15.7 μm^2 per micrograph) to compare the density of parallel fiber to Purkinje cell synapses.

***In vitro* electrophysiology.** Mice (10–25-weeks-old) were anaesthetized with isoflurane (IVAX Pharmaceuticals) and parasagittal slices (250–300 μm) were cut from the cerebellar vermis/paravermis (HM 650V, Microm International GmbH) as described previously[16]. Slices were transferred to a submerged recording chamber and perfused (1.5–2.5 ml min^{-1}) with an external solution containing 125 mM NaCl, 2.5 mM KCl, 2 mM CaCl$_2$, 1 mM MgCl$_2$, 25 mM NaHCO$_3$, 1.25 mM NaH$_2$PO$_4$ and 25 mM D-glucose, pH 7.4 when bubbled with 95% O$_2$ and 5% CO$_2$. Patch-clamp recordings were made with Axopatch 200A or 200B amplifiers (Molecular Devices) from Purkinje cells visualized under infrared differential interference contrast optics (Zeiss Axioscop or Olympus BX51 WI). Whole-cell and single-channel currents were recorded

at 23–26 °C. Simple spike activity was recorded at both 23–26 °C and 34 ± 2 °C in loose cell-attached mode with external solution in the recording pipette. Firing was recorded in voltage- or current-clamp with the pipette current set to zero[12].

For whole-cell and loose cell-attached recordings, pipettes were pulled from thin-walled borosilicate glass tubing (1.5 mm outer diameter, 1.17 mm inner diameter, G150TF-3, Warner Instruments). For patch recordings, thick-walled borosilicate glass tubing (1.5 mm outer diameter, 0.86 mm inner diameter, GC-150F, Harvard Apparatus) was used. Pipettes were coated with Sylgard resin (Dow Corning 184) and fire polished to give a final resistance of 2–6 MΩ (whole cell and loose cell attached) or 10–15 MΩ (single channel). The internal solution contained 140 mM CsCl, 4 mM NaCl, 0.5 mM CaCl$_2$, 10 mM *N*-2-hydroxyethylpiperazine-*N*′-2-ethanesulphonic acid (HEPES), 5 mM ethylene-glycol-bis (β-aminoethylether)-*N*,*N*,*N*′,*N*′-tetraacetic acid (EGTA) and 2 mM Mg-ATP, pH 7.3 with CsOH. Ionotropic glutamate receptors were blocked with 10 μM D-AP5 and 5 μM CNQX. mIPSCs were recorded in the presence of 0.5–1 μM TTX.

Parallel fiber–evoked responses were recorded in loose cell-attached mode during molecular layer stimulation (a glass pipette containing external solution was placed in fixed position ~100–150 μm from the recorded Purkinje cell soma). Stimuli of 5–10 V and 100-μs duration were delivered at 0.5 Hz (Digitimer DS2 isolated stimulator). Recordings were made in the absence of drugs. The effect of GABA$_A$ receptor blockade was tested using SR-95531 (40 μM). In all cases tested, 2,3-dioxo-6-nitro-1,2,3,4-tetrahydrobenzo[f]qui-noxaline-7-sulfonamide (NBQX) completely blocked evoked responses (data not shown).

Long-term plasticity at parallel fiber–Purkinje cell synapses was examined as previously described[41]. We cut 200-μm-thick parasagittal slices in ice-cold artificial cerebrospinal fluid (containing 124 mM NaCl, 5 mM KCl, 1.25 mM Na$_2$PO$_4$, 2 mM MgSO$_4$, 2 mM CaCl$_2$, 26 mM NaHCO$_3$ and 15 mM D-glucose, bubbled with 95% O$_2$ and 5% CO$_2$). Experiments were carried out at 23–26 °C with GABA$_A$ receptors blocked (100 μM picrotoxin). Whole-cell patch-clamp recordings of Purkinje cells were performed using an EPC-10 amplifier (HEKA Electronics). Pipette resistance was 4–5 MΩ when filled with intracellular solution containing 120 mM potassium gluconate, 9 mM KCl, 10 mM KOH, 3.48 mM MgCl$_2$, 4 mM NaCl, 10 mM HEPES, 4 mM Na$_2$ATP, 0.4 mM Na$_3$GTP and 17.5 mM sucrose (pH 7.25). LTP was induced by parallel fiber stimulation at 1 Hz for 5 min in current-clamp mode and measured by test responses recorded in voltage-clamp mode. LTD was induced using combined parallel and climbing fiber stimulation[41]. All drugs were obtained from Tocris Bioscience, Ascent Scientific or Sigma.

Eye-movement recordings. Mice (12–30-weeks-old) were surgically prepared under general anesthesia with isoflurane. A construct with two nuts was attached to the frontal and parietal bones using Optibond (Kerr) and Charisma (Heraeus Kulzer). After 5 d of recovery, mice were placed in a restrainer, with their heads bolted to a bar. The restrainer was fixed onto the turntable. A cylindrical screen (diameter 63 cm) with a random-dotted pattern (each element 2°) surrounded the turntable (diameter 60 cm). OKR and visual VOR were evoked by independently rotating the screen and turntable (5° amplitude at different frequencies, AC servo-motors, Harmonic Drive AG). The table and drum position were measured by potentiometers and the signal was digitized (CED) and stored for off-line analysis. Eye movements were recorded using an infrared CCD camera fixed to the turntable (240 Hz, ISCAN). Video calibrations and eye movement computations were carried out as described previously[27,49].

***In vivo* electrophysiology.** Mice (15–40-weeks-old) were surgically prepared under general anesthesia by mounting a pedestal as described above[27]. A recording chamber was built around craniotomies in left and right occipital bones. Extracellular Purkinje cell activity was recorded using borosilicate glass electrodes (outer diameter = 2.0 mm, inner diameter = 1.16 mm, 2 M NaCl, 4–8 MΩ). Electrodes were advanced by a hydraulic micro-drive (Narishige). Recordings were made from left and right Crus I and II, paramedian lobule, and (para)flocculus (recordings during optokinetic stimulation were from floccular Purkinje cells). Purkinje cells were identified by the brief pause in simple-spike activity following each complex spike. The raw signal was

amplified, filtered (CyberAmp, CED), digitized (CED) and stored for off-line analysis. Following each recording session, the brain was covered with grami-cidin-containing ointment and the chamber was sealed with bone wax.

Data analysis. During *in vitro* experiments, signals were recorded onto digital audiotape (DTR-1204, BioLogic, DC to 20 kHz); for analysis, replayed signals were filtered at 2 or 5 kHz (whole-cell and single-channel or loose cell-attached recordings, respectively, −3 dB, 8-pole lowpass Bessel) and digitized at 10 kHz (Digidata 1200, Axotape, Molecular Devices). mIPSCs were detected using a scaled template detection method[50] implemented in IGOR Pro 5.0 (Wave-metrics) with NeuroMatic 1.91 (http://www.neuromatic.thinkrandom.com)[16]. The decay of synaptic currents is best described by the sum of two exponential functions according to

$$y = A_1 \exp\left(\frac{-(x - x_0)}{\tau_1}\right) + A_2 \exp\left(\frac{-(x - x_0)}{\tau_2}\right)$$

where x_0 is the decay onset, τ_1 and τ_2 are the decay time constants of the fast and slow components, and A_1 and A_2 are their respective amplitudes. The weighted time constant of decay (τ_w) was calculated according to

$$\tau_w = \tau_1\left(\frac{A_1}{A_1 + A_2}\right) + \tau_2\left(\frac{A_2}{A_1 + A_2}\right)$$

Purkinje cell simple spikes were detected by threshold crossing. ISIs and PSTHs were generated using NeuroMatic and IGOR Pro 5.0 for spontaneous and parallel fiber–evoked responses, respectively. To determine the number of extra spikes evoked by stimulation, we integrated PSTHs. A linear fit to the prestimulus section was extrapolated over the full duration of the integral and subtracted to yield the cumulative spike probability corrected for baseline firing[7]. The number of additional spikes evoked by each stimulus was determined by averaging over a 0–60-ms period.

Off-line analysis of eye movements and *in vivo* recordings was performed in Matlab (MathWorks)[27]. Gain and phase of eye movements were determined by fitting sine functions to the slow-phase eye velocity traces. Gain was computed as the ratio of eye velocity to stimulus velocity, whereas phase was expressed as the difference (in degrees) between eye velocity and stimulus velocity traces.

In vivo simple spikes and complex spikes were discriminated using custom-made routines based on principal component analysis. Simple-spike PSTHs (100 bins per cycle) were compiled at each stimulus frequency and fitted by a sine function. Epochs containing quick phases were deleted from the trace (−50 to +150 ms). Modulation was calculated by dividing the amplitude of the fitted sine wave by its offset. Phase difference was calculated as the difference between the phase of the fitted sine wave and the optokinetic stimulus.

Models and simulations. A phenomenological model of an idealized VOR circuit was created to elucidate the potential role of vestibular nuclei in a phase adaptation procedure. Elements in the VOR circuit were characterized by the gain and phase of their sinusoidal modulation, which define the coordinates of a position on a polar plot. Plasticity rules were employed phenomenologically, as exponential decay of the modulation along a trajectory in a polar plot, with the target gain and phase (new position in the polar plot) being defined by the vestibular mismatch. Equations were solved numerically using Matlab. See **Supplementary Data** for details.

Statistical analyses. Statistical tests were performed with GraphPad (Prism 3.0, GraphPad Software) or with SPSS 11 (SPSS). Unless stated otherwise, data were compared with two-tailed paired or unpaired Student's *t* tests, as appropriate. We also used two-way repeated-measures ANOVA and, where data were non-normally distributed (Shapiro-Wilk test), the Mann-Whitney *U* test. The level of significance was set at $P < 0.05$.

49. Stahl, J.S., van Alphen, A.M. & De Zeeuw, C.I. A comparison of video and magnetic search coil recordings of mouse eye movements. *J. Neurosci. Methods* **99**, 101–110 (2000).
50. Clements, J.D. & Bekkers, J.M. Detection of spontaneous synaptic events with an optimally scaled template. *Biophys. J.* **73**, 220–229 (1997).